CORONAVIRUS

JAK inhibition reduces SARS-CoV-2 liver infectivity and modulates inflammatory responses to reduce morbidity and mortality

Justin Stebbing[1]*[†], Ginés Sánchez Nievas[2†], Marco Falcone[3†], Sonia Youhanna[4†], Peter Richardson[5], Silvia Ottaviani[1], Joanne X. Shen[4], Christian Sommerauer[6], Giusy Tiseo[3], Lorenzo Ghiadoni[3], Agostino Virdis[3], Fabio Monzani[3], Luis Romero Rizos[7,8], Francesco Forfori[9], Almudena Avendaño Céspedes[7,8], Salvatore De Marco[10], Laura Carrozzi[9], Fabio Lena[11], Pedro Manuel Sánchez-Jurado[7,8], Leonardo Gianluca Lacerenza[11], Nencioni Cesira[12], David Caldevilla Bernardo[13], Antonio Perrella[12], Laura Niccoli[14], Lourdes Sáez Méndez[15], Daniela Matarrese[16], Delia Goletti[17], Yee-Joo Tan[18], Vanessa Monteil[19], George Dranitsaris[20], Fabrizio Cantini[14], Alessio Farcomeni[21], Shuchismita Dutta[22], Stephen K. Burley[22], Haibo Zhang[23], Mauro Pistello[24], William Li[25], Marta Mas Romero[7], Fernando Andrés Pretel[26], Rafaela Sánchez Simón-Talero[27], Rafael García-Molina[7], Claudia Kutter[6], James H. Felce[28], Zehra F. Nizami[28], Andras G. Miklosi[28], Josef M. Penninger[29,30], Francesco Menichetti[3‡], Ali Mirazimi[18‡], Pedro Abizanda[7,8‡], Volker M. Lauschke[4*‡]

Using AI, we identified baricitinib as having antiviral and anticytokine efficacy. We now show a 71% (95% CI 0.15 to 0.58) mortality benefit in 83 patients with moderate-severe SARS-CoV-2 pneumonia with few drug-induced adverse events, including a large elderly cohort (median age, 81 years). An additional 48 cases with mild-moderate pneumonia recovered uneventfully. Using organotypic 3D cultures of primary human liver cells, we demonstrate that interferon-α2 increases ACE2 expression and SARS-CoV-2 infectivity in parenchymal cells by greater than fivefold. RNA-seq reveals gene response signatures associated with platelet activation, fully inhibited by baricitinib. Using viral load quantifications and superresolution microscopy, we found that baricitinib exerts activity rapidly through the inhibition of host proteins (numb-associated kinases), uniquely among antivirals. This reveals mechanistic actions of a Janus kinase-1/2 inhibitor targeting viral entry, replication, and the cytokine storm and is associated with beneficial outcomes including in severely ill elderly patients, data that incentivize further randomized controlled trials.

INTRODUCTION

The novel severe acute respiratory syndrome coronavirus 2 (SARS-CoV-2) pandemic has become the biggest public health challenge of this century with more than 1 million fatalities and 34 million cases of coronavirus disease 2019 (COVID-19) across all countries in the first 10 months since it emerged (1–4). It is essential that more effective treatments are found before a vaccine is developed and made widely available (5, 6). We previously reported that use of artificial intelligence (AI) based on a knowledge graph of more than 1 billion relationship edges enabled the rapid identification of the once daily orally administered drug, baricitinib, approved as a treatment for adult rheumatoid arthritis (RA), as a potential therapeutic (7–11). Baricitinib was predicted to have a dual mode of action, reducing viral infectivity through the inhibition of numb-associated kinases (NAKs) and, thus, viral endocytosis and its better known well-described anti-inflammatory mechanism through blockade of Janus kinase 1/2 (JAK1/2) (12–14).

[1]Department of Surgery and Cancer, Imperial College, London, UK. [2]Department of Rheumatology, Complejo Hospitalario Universitario de Albacete, Albacete, Spain. [3]Department of Clinical and Experimental Medicine, University of Pisa, Pisa, Italy. [4]Department of Physiology and Pharmacology, Karolinska Institutet, Stockholm, Sweden. [5]BenevolentAI, Maple Street, London, UK. [6]Department of Microbiology, Tumor, and Cell Biology, Karolinska Institutet, Science for Life Laboratory, Solna, Sweden. [7]Department of Geriatric Medicine, Complejo Hospitalario Universitario de Albacete, Albacete, Spain. [8]CIBERFES, Ministerio de Economía y Competitividad, Madrid, Spain. [9]Department of Surgical, Medical and Molecular Pathology and Critical Care Medicine, Pisa, University of Pisa, Italy. [10]Department of Internal Medicine, Azienda Ospedaliera Universitaria Pisana, Pisa, Italy. [11]Department of Pharmaceutical Medicine, Misericordia Hospital, Grosseto, Italy. [12]Department of Medicine, Misericordia Hospital, Grosseto, Italy. [13]Department of Radiology, Complejo Hospitalario Universitario de Albacete, Albacete, Spain. [14]Department of Rheumatology, Hospital of Prato, Prato, Italy. [15]Department of Internal Medicine, Complejo Hospitalario Universitario de Albacete, Albacete, Spain. [16]Hospital Network ASL Toscana Centro, Toscana, Italy. [17]Department of Epidemiology and Preclinical Research, National Institute for Infectious Diseases–IRCCS, Rome, Italy. [18]University of Singapore, Infectious Diseases Programme, Immunology Programme, Department of Microbiology and Immunology, Yong Loo Lin School of Medicine, National University of Singapore and Institute of Molecular and Cell Biology (IMCB), A*STAR (Agency for Science, Technology and Research), Singapore, Singapore. [19]Karolinska Institutet, Department of Laboratory Medicine, Unit of Clinical Microbiology, and SE-17177, Stockholm, Sweden. [20]Department of Hematology, School of Medicine, University of Ioannina, Ioannina, Greece. [21]Department of Economics and Finance, University of Rome Tor Vergata, Rome Italy. [22]RCSB Protein Data Bank, Rutgers, The State University of New Jersey, Piscataway, NJ, USA. [23]Departments of Anesthesia, Medicine, and Physiology, University of Toronto, Toronto, ON, Canada. [24]Virology Unit, Department of Translational Research, University of Pisa, Pisa, Italy. [25]The Angiogenesis Foundation, Cambridge, MA, USA. [26]Department of Statistics, Complejo Hospitalario Universitario de Albacete, Albacete, Spain. [27]Department of Pneumology, Complejo Hospitalario Universitario de Albacete, Albacete, Spain. [28]Oxford Nanoimaging, Oxford, UK. [29]Institute of Molecular Biotechnology of the Austrian Academy of Sciences, Vienna, Austria. [30]Department of Medical Genetics, Life Science Institute, University of British Columbia, Vancouver, BC, Canada. [31]National Veterinary Institute, Uppsala, Sweden.

*Corresponding author. Email: j.stebbing@imperial.ac.uk (J.S.); volker.lauschke@ki.se (V.M.L.)
†These authors contributed equally to this work.
‡These authors contributed equally to this work.

In severe cases, the so-called "cytokine storm" can result in profound lung damage and the development of acute respiratory distress syndrome (ARDS), the leading cause of death in COVID-19 (15, 16). SARS-CoV-2 infection also results in damage to many other organs including the kidneys, brain, and vasculature via mechanisms including endothelial cell disruption and intussusceptive angiogenesis (17, 18). Plasma levels of the proinflammatory cytokine interleukin-6 (IL-6) signaling predominantly through JAK/STAT (signal transducer and activator of transcription) have been reported to be a prognostic indicator of mortality (19, 20), and using samples from a randomized phase 2b trial in RA (4), we demonstrated that baricitinib reduces IL-6 levels in a dose-dependent manner (21), the first time this has been shown in patients. Therapeutics capable of clearing the virus and reducing the cytokine-mediated inflammation may be beneficial. Purported antiviral agents have, at best, a small impact on disease remission in hospitalized patients and, in some cases, show no differences in viral loads compared to control arms (22). Dexamethasone, known to modulate inflammation-mediated lung injury, resulted in lower mortality among those who were receiving either invasive mechanical ventilation or oxygen alone at randomization (23). In many cases, patients are unable to withstand the exuberant inflammation associated with ARDS. Furthermore, high viral loads cause disseminated end-organ compromise through vascular endotheliitis, thrombosis, and other associated effects (17, 24).

In this situation, an assessment of the efficacy of baricitinib would include demonstration of reduced viral infectivity and associated end-organ damage and control of the excessive cytokine-mediated inflammation. Here, we explore the clinical effect of baricitinib therapy patients and matched controls from two European cohorts. Since COVID-19 is associated with multisystem organ damage, we also investigated whether the cytokine-mediated inflammation could induce the expression of the SARS-CoV-2 receptor angiotensin-converting enzyme 2 (ACE2) (25, 26) in extrapulmonary systems. We show that type-1 interferons (IFNs), specifically IFN-α2, whose levels are increased in patients with severe COVID-19 (27), increase ACE2 expression in three-dimensional (3D) cultures of primary human liver cells, resulting in increased viral load, and that this induction is fully inhibited by clinically relevant concentrations of baricitinib.

RESULTS
Clinical results
A total of 601 patients were enrolled in the University of Pisa ($n = 179$) and Albacete Hospital ($n = 422$) cohorts, between mid-March and mid-April 2020, when these regions were the global epicenters of the pandemic, under severe capacity constraints. Of these, 37 patients were treated with baricitinib in the Pisa cohort and 46 were treated in the Albacete cohort, all of European descent; eighty-three controls were included using propensity score–matching systems, both in the Italian and in the Spanish cohorts, as per the CONSORT diagram (Fig. 1).

Tables 1 and 2 present baseline data of participants from Pisa and Albacete, respectively, showing clinical characteristics immediately following admission, and Table 3 presents propensity score–matched population data from both sites, comprising the group taking baricitinib and the control group. Male sex was predominant, and the Albacete patients were older than those from Pisa (80.9 versus 66.0 years) in treated groups. Most individuals received concomitant "antiviral therapy" with hydroxychloroquine and lopinavir/ritonavir,
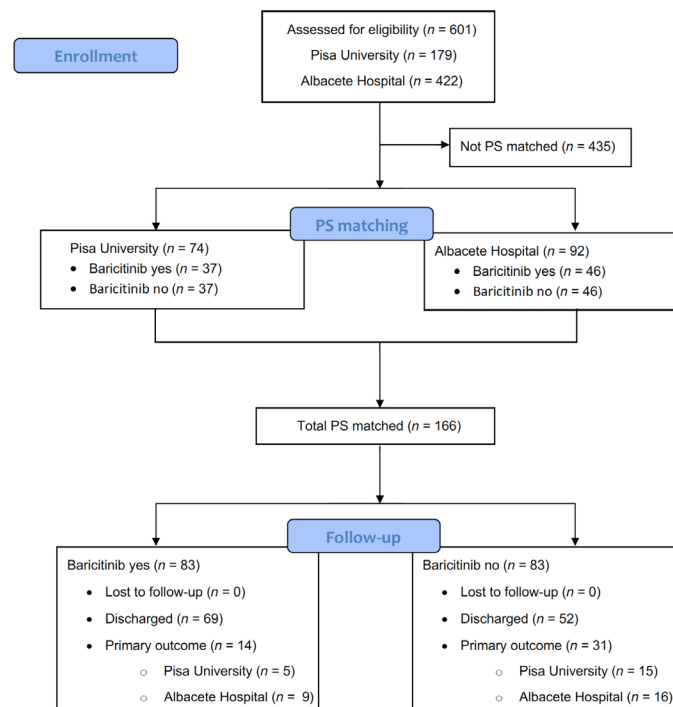

Fig. 1. CONSORT flow diagram for University of Pisa and Albacete Hospital cohorts. PS, propensity score.

antibiotics, corticosteroids, and low–molecular weight heparin (LMWH). In the merged matched population, the primary composite end point of death or invasive mechanical ventilation occurred in 14 (16.9%) patients in the baricitinib-treated group compared to 29 (34.9%) in the control group ($P < 0.001$) (Table 3). In the multivariate Cox regression analysis adjusted for all the covariates included in the matching of the two cohorts, baricitinib was independently associated as a protective variable with the primary outcome [hazard ratio (HR) 0.29; 95% confidence interval (CI) 0.15 to 0.58; $P < 0.001$] (Table 4). Figure 2 presents the Kaplan-Meier curves for the primary outcome in the treated and control groups in the merged cohorts. Baricitinib's favorable effect appeared "early" and was maintained until termination of the follow-up ($P < 0.0001$). Further analyses including only participants who received five or more baricitinib doses yielded similar results as those presented. Analyses of the propensity score–matched cohorts from the University of Pisa (fig. S3A) and Albacete Hospital (fig. S3B) are shown independently. Similar curves and statistics can be observed, compared with the final merged cohort (Fig. 2).

Safety issues with baricitinib
A major role of observational studies is to provide relevant information regarding toxicity. Seven (19%) individuals from Pisa reported transaminitis [2× to 5× upper limit of normal (ULN)] within 72 hours of commencing baricitinib, leading to cessation of the drug in four of these patients. In three patients and in our previously published small series (21), we continued to treat despite this and the liver function abnormalities self-resolved. One patient developed a severe lymphocytopenia (<500 cells/mm^3) during treatment, leading to drug discontinuation. A total of five (14%) individuals from Pisa developed infectious complications during baricitinib treatment as follows: one bacteremia due to *Enterococcus faecalis* arising from the urinary tract, two

Table 1. Characteristics of patients receiving or not receiving baricitinib in the unmatched and matched study population from the University of Pisa (Italy). All data are medians with the interquartile range or number of participants (%). COPD, chronic obstructive pulmonary disease; PaO₂/FiO₂, ratio of arterial oxygen partial pressure to fractional inspired oxygen; ALT, alanine aminotransferase; ARB, angiotensin-receptor blocker; AST, aspartate aminotransferase; SOFA, sequential organ failure assessment; ULN, upper limit of normal.

	Baricitinib group ($n = 37$)	Control group ($n = 142$)	PS matched control group ($n = 37$)
Age	66.0 (48.0–84.0)**	76.5 (62.5–83)**	65 (40–90)
Male sex	27 (73)	95 (66.9)	26 (70.3)
Interval between symptom onset and admission	6 (3.5–9)	7 (3–8)	7 (4–7.5)
Coexisting conditions			
Hypertension	16 (43.2)	79 (55.9)	18 (48.6)
Cardiovascular disease	9 (24.3)	56 (39.4)	6 (16.2)
Solid cancer	6 (16.2)	22 (15.5)	9 (24.3)
Diabetes	7 (18.9)	32 (22.5)	8 (21.6)
COPD	1 (2.7)*	27 (19.0)*	0 (0.0)
Chronic kidney failure	2 (5.4)	16 (11.3)	1 (2.7)
Charlson comorbidity index	2 (0–4)	2 (1–5)	1 (0–6)
Medications at baseline			
ACE inhibitor or ARB	9 (24.3)	43 (30.4)	9 (24.3)
Direct oral anticoagulant or warfarin	5 (13.5)	24 (16.9)	1 (2.7)
SOFA score	3 (1–5)	3 (2–4)	3 (2–4)
Baseline PaO₂/FiO₂	242 (143–341)	254 (200–298)	252 (169–335)
Noninvasive mechanical ventilation	17 (45.9)***	19 (13.4)***	13 (35.1)
Baseline laboratory tests			
C-reactive protein (mg/dl)	5.7 (0.0–18.0)	8.3 (3.7–16.1)	11.2 (0.0–25.4)
Lymphocyte count	1010 (400–1620)	830 (580–1160)	740 (145–1335)
ALT (U/liter)	39 (13–65)	25 (16–45)	28 (0–58)
AST (U/liter)	43 (12–74)	33 (24–50)	32 (10–54)
ALT > 3× ULN	1 (2.7%)	8 (5.6%)	1 (2.7%)
AST > 3× ULN	1 (2.7%)	11 (7.7%)	2 (5.4%)
Total bilirubin (mg/dl)	0.51 (0.31–0.71)	0.49 (0.35–0.77)	0.48 (0.08–0.88)
Concomitant treatment			
Hydroxychloroquine	34 (91.9)*	102 (71.8)*	34 (91.9)
Other antibiotics	33 (89.2)	109 (76.8)	34 (91.9)
Proteases inhibitors	30 (81.1)*	89 (62.7)*	29 (78.4)
LMWH (enoxaparin)	36 (97.3)***	98 (69)***	36 (97.3)
Steroids	27 (73.0)**	65 (45.8)**	28 (75.7)
Primary outcome	5 (13.5)***	66 (46.5)***	13 (35.1)*
Invasive mechanical ventilation	4 (10.8)	19 (13.4)	9 (24.3)
Died without intubation	1 (2.7)	47 (33.1)	4 (5.4)

*$P < 0.05$ **$P < 0.01$ ***$P < 0.001$

episodes of central venous catheter–related bacteremia due to coagulase-negative staphylococci, one urinary tract infection by New Delhi metallo-beta-lactamase (NDM)–producing *Klebsiella pneumoniae*, and one severe facial herpes simplex infection. In the unmatched control group, a total of 21 (14.8%) patients developed an infection: 8 bloodstream infections, 8 urinary tract infections, and 5 with pneumonia. In the propensity score–matched control group, six

(16.2%) episodes of infection occurred: one bacteremia due to *Enterobacter aerogenes* arising from the urinary tract, one bacteremia by NDM-producing *K. pneumoniae*, three urinary tract infections (due to *Escherichia coli*, *E. faecalis*, and *K. pneumoniae*), and one pneumonia by *Pseudomonas aeruginosa*.

Apart from transaminitis, adverse events were difficult to ascribe to baricitinib because of rapidly evolving clinical/capacity constraints.

Table 2. Characteristics of patients receiving or not receiving baricitinib in the unmatched and matched study population from the Albacete Hospital (Spain). IMV, invasive mechanical ventilation. All data are means (SD) or number of participants (%).

	Baricitinib group (n = 46)	Control group (n = 376)	PS matched control group (n = 46)
Age	80.9 (5.8)	82.7 (6.3)	80.6 (6.3)
Male sex	30 (65.2)	201 (53.5)	30 (65.2)
Interval between symptom onset and admission	7.4 (5.2)	7.3 (4.9)	7.3 (5.1)
Coexisting conditions			
Hypertension	34 (73.9)	296 (78.7)	35 (76.1)
Cardiovascular disease	18 (39.1)	167 (44.4)	15 (32.6)
Solid cancer	2 (4.3)	20 (5.3)	1 (2.2)
Diabetes	21 (45.7)	139 (37.0)	14 (30.4)
COPD	11 (23.9)	84 (22.3)	12 (26.1)
Chronic kidney failure	5 (10.9)	64 (17.0)	6 (13.0)
Charlson comorbidity index	2.9 (2.3)	2.0 (1.9)	3.2 (2.8)
Medications at baseline			
ACE inhibitor or ARB	24 (52.2)	196 (52.3)	26 (56.5)
Direct oral anticoagulant or warfarin	8 (17.4)	65 (17.3)	4 (8.7)
Antiaggregants	14 (30.4)	121 (32.2)	15 (32.6)
Statins	23 (50.0)	158 (42.0)	21 (45.7)
Insulin	9 (19.6)	42 (11.2)	4 (4.3)
Oral hypoglycemic agents	15 (32.6)	109 (29.0)	13 (28.3)
Antidepressants	10 (21.7)	123 (32.7)	11 (23.9)
Inhaled therapy for COPD	12 (26.1)	95 (25.3)	15 (32.6)
Baseline PaO_2/FiO_2	284 (109)	280 (107)	282 (96)
Baseline laboratory tests			
D-dimer (µg/liter)	6944 (18,052)	6182 (26,894)	5443 (16,872)
Lactate dehydrogenase (U/liter)	387 (136)	372 (288)	370 (166)
C-reactive protein (mg/liter)	147.2 (98.6)	137.6 (118.0)	141.8 (145.8)
Ferritin (ng/ml)	1357 (1094)**	878 (975)**	1039 (927)
Leucocyte count (per µl)	9414 (4790)	8986 (4711)	7690 (3675)
Lymphocyte count (per µl)	987 (905)	967 (777)	934 (517)
Hemoglobin (g/dl)	13.7 (2.1)	13.2 (2.1)	13.7 (3.2)
Fibrinogen (mg/dl)	395 (78)	378 (175)	375 (70)
Creatinine (mg/dl)	1.2 (0.5)	1.3 (0.91)	1.1 (0.5)
AST (U/liter)	35.5 (23.4)	41.4 (40.3)	40 (46)
Gamma-glutamyltransferase (U/liter)	63.3 (49.5)	54.2 (74.3)	65.5 (119.2)
ALT (U/liter)	33.8 (25.3)	30.8 (57.3)	31.0 (25.5)
ALT (U/liter) after treatment, at discharge	47.5 (45.8)	–	–
ALT > 2× ULN after treatment, at discharge	5 (9.1)	–	–
ALT > 3× ULN after treatment, at discharge	3 (5.5)	–	–
Chest x-ray			
Interstitial pattern	46 (100)	345 (93.0)	44 (95.7)
Opacities	38 (82.6)*	233 (63.7)*	32 (69.6)
Severity score	3.4 (2.1)**	2.2 (2.2)**	2.4 (2.1)
Concomitant treatment			

Continued on the next page

	Baricitinib group (*n* = 46)	Control group (*n* = 376)	PS matched control group (*n* = 46)
Hydroxychloroquine	45 (97.8)*	321 (85.4)*	46 (100)
Antibiotics	46 (100)	365 (97.1)	45 (97.8)
Lopinavir/ritonavir	39 (84.8)	288 (76.8)	42 (91.3)
LMWH (enoxaparin)	46 (100)**	322 (85.6)**	46 (100)
Glucocorticoids	44 (95.7)***	266 (70.7)***	42 (91.3)
Anakinra	18 (39.1)***	29 (7.7)***	10 (21.7)
Primary outcome (mortality or IMV)	9 (19.6)**	157 (41.8)**	16 (34.8)

*$P < 0.05$ **$P < 0.01$ ***$P < 0.001$

Table 3. Common characteristics of patients receiving or not receiving baricitinib in the propensity score–matched populations from the University of Pisa and the Albacete Hospital. PS, propensity score matching. All data are means (SD) or number of participants (%).

	Baricitinib group (*n* = 83)	PS control group (*n* = 83)
Age	74.0 (12.5)	74.1 (13.6)
Male sex	43 (51.8)	42 (50.6)
Coexisting conditions		
Hypertension	50 (60.2)	53 (63.9)
Cardiovascular disease	27 (32.5)	21 (25.3)
Solid cancer	8 (9.6)	10 (12.0)
Diabetes	28 (33.7)	22 (26.5)
COPD	12 (14.5)	12 (14.5)
Chronic kidney failure	7 (8.4)	7 (8.4)
Charlson comorbidity index	2.7 (2.3)	2.8 (2.7)
Medications at baseline		
ACE inhibitor or ARB	33 (39.8)	35 (42.2)
Baseline PaO_2/FiO_2	268 (101)	266 (86)
Baseline laboratory tests		
C-reactive protein (mg/liter)	86.0 (100.6)	82.2 (123.9)
Lymphocyte count (per µl)	1052 (831)	40 (46)
ALT (U/liter)	38.7 (26.5)	34.6 (29.9)
Concomitant treatment		
Hydroxychloroquine	79 (95.2)	80 (96.4)
Antibiotics	79 (95.2)	79 (95.2)
Lopinavir/ritonavir	69 (83.1)	71 (85.5)
LMWH	82 (98.8)	82 (98.8)
Glucocorticoids	71 (85.5)	70 (84.3)
Primary outcome	14 (16.9)*	29 (34.9)*
Time to outcome	19.9 (9.1)**	13.1 (9.7)**

*$P < 0.01$ **$P < 0.001$

We did not observe any signs of coagulopathy or thrombosis caused by baricitinib in any of our patients, although this has been described as a potential toxicity associated with longer-term use in RA (*12–14*). However, most were anticoagulated with LMWH.

Table 4. Multivariate Cox regression analyses for the primary outcome in the propensity score–matched populations from the University of Pisa and the Albacete Hospital. Selection bias was addressed by propensity score analysis. Briefly, this is a two-phase technique used to estimate a treatment effect in comparative groups selected by nonrandom means. In the first phase of a propensity score analysis, variables that influence selection to group assignment are used to model the probability of receiving treatment (or of being in the reference group, in this case, the baricitinib group). The resulting probability is the propensity score. In the second phase, the propensity score is used to adjust for preexisting group differences in the analysis of the relevant outcomes. There are several ways to use propensity scores such as stratification variables, matching patients on the basis of their propensity score, or their use as a weighting or adjustment variable during multivariate analysis. In the current study, each baricitinib patient was matched to a control patient on the basis of comparable propensity scores. Assuming that all relevant covariates are included in the propensity score model, the group effect observed in a propensity score analysis represents an unbiased estimate of the true treatment effect.

|	HR (95% CI)	*P*
Baricitinib	0.29 (0.15–0.58)	0.0001
Age	1.01 (0.98–1.04)	0.470
Male sex	1.13 (0.54–2.34)	0.750
Hypertension	1.31 (0.52–3.32)	0.572
Diabetes	0.51 (0.23–1.17)	0.113
Chronic obstructive lung disease	0.51 (0.17–1.54)	0.230
Cardiovascular disease	1.41 (0.68–2.92)	0.351
Chronic kidney disease	1.45 (0.51–4.15)	0.491
Solid cancer	1.18 (0.49–2.87)	0.709
Charlson comorbidity index	1.03 (0.90–1.17)	0.680
Baseline PaO_2/FiO_2	1.00 (1.00–1.00)	0.823
Lymphocyte count (per µl)	1.00 (1.00–1.00)	0.657
ALT	1.01 (1.00–1.03)	0.026
Hydroxychloroquine	2.77 (0.28–27.41)	0.384
Lopinavir/ritonavir	1.18 (0.38–3.61)	0.776
Glucocorticoids	1.79 (0.60–5.34)	0.299
LMWH	0.10 (0.01–1.33)	0.081
Antibiotics	2.34 (0.29–18.90)	0.427
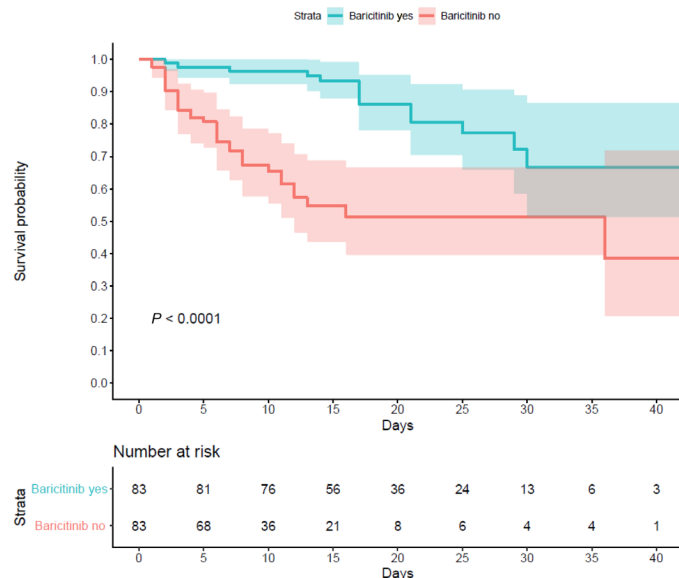
Fig. 2. Kaplan-Meier analysis of the propensity score–matched cohorts from Pisa University and Albacete Hospital cohorts.

In the Spanish cohort, a transaminitis of 2× ULN was observed after baricitinib treatment in eight (17%) patients and at 3× ULN in four (9%) patients; the drug was not stopped in any individual based on this, and abnormalities normalized despite the continuation of treatment. Other adverse events probably or possibly related to baricitinib were observed in nine (20%) patients: two oral candidiasis, one bacteremia for *Enterococcus faecium*, one bacterial pneumonia with negative cultures, three new atrial fibrillation (all had previous heart disease), one hypertensive episode, one episode of heart failure in the presence of known heart disease, one case of urinary obstruction, one episode of diarrhea, and one gastrointestinal bleed in an individual with gastric malignancy. In the unmatched control group from Albacete (n = 376), we observed 17 (4.5%) urinary tract infections and one herpes zoster reactivation. Other complications were gastrointestinal (nausea, vomiting, or diarrhea) in 30.7%, hepatic in 4.5%, renal in 21.1%, neurologic in 9.8%, cutaneous in 4%, and arrhythmias in 5.1%.

IFNs sensitize 3D primary human liver cultures to SARS-CoV-2 infections by inducing ACE2

Organotypic 3D cultures of primary human liver cells are susceptible to infection with SARS-CoV-2 as previously reported (*21*), with virus signals being enriched in proximity to ACE2 proteins (Fig. 3A). Thus, we evaluated the effect(s) of cytokines on ACE2 expression. To evaluate cytokine effects on human liver cells, we focused on IFNs (IFN-α2, IFN-β, and IFN-γ), interleukins (IL-1β, IL-6, IL-10, and IL-18), and tumor necrosis factor–α (TNFα), serum levels of which are increased in patients with moderate-to-severe disease (*15, 16, 28*). We detected greater than fivefold induction of ACE2 expression after 16 hours of exposure with IFN-α2 and IFN-β, whereas IFN-γ, TNFα, and the other interleukins tested did not induce ACE2 in liver microtissues (Fig. 3B). As IFN-α2 serum levels in patients exceed those of IFN-β, we focused our subsequent analyses on IFN-α2. Coexposure of liver spheroids to IFN-α2 in combination with other cytokines did not significantly amplify IFN-mediated ACE2 induction (Fig. 3C). On the basis of these data, we thus hypothesized that increased levels of

IFN-α2 in patients with severe SARS-CoV-2 infection can stimulate ACE2 expression in parenchymal cells and further increase virulence.

Next, we evaluated the effects of IFN-α2–mediated induction of ACE2 on viral load and found that IFN-α2 increased viral copy numbers in 3D organotypic liver cultures by approximately twofold (Fig. 3D). Exposure to therapeutically relevant concentrations of baricitinib (800 nM) fully abolished ACE2 induction by IFN-α2 and efficiently blocked the increased infectivity in cytokine-treated 3D liver microtissues even beyond the levels observed in non–cytokine-exposed samples (Fig. 3, D and E), in agreement with our previous report (*21*). In contrast, in lung organoids, IFN-α2 did not induce ACE2 even at higher concentrations and had opposite, i.e., mild antiviral, effects (50 ng/ml compared to 10 ng/ml for liver spheroids; Fig. 3, F and G), suggesting that IFN effects differ between pulmonary organs and liver. Furthermore, baricitinib did not reduce viral levels in monkey kidney epithelial cells (Vero cells) and human adenocarcinomic alveolar basal epithelial cells (A549 cells) (fig. S4). These results demonstrate that infection and replication mechanisms in primary cells and cell lines are distinctly different and incentivize the use of organotypic culture systems for studies of infectious disease biology.

Baricitinib efficiently blocks IFN signaling

To gain a detailed understanding of the molecular effects of baricitinib, we sequenced primary liver spheroids using RNA sequencing (RNA-seq), resulting in the first comprehensive map of IFN response genes in human hepatocytes. In infected and noninfected liver spheroids, IFN-α2 significantly induced a total of 407 and 696 genes, respectively [log₂ fold change (FC) > |1| and false discovery rate (FDR) < 0.05; Fig. 4A]. Genes that were differentially expressed irrespective of infection (n = 271) were strongly enriched in viral defense pathways, antigen presentation, and endosomal trafficking (Fig. 4B). IFN strongly regulated genes associated with platelet activation (*29*), but this effect was blunted by viral infection, demonstrating intricate pathway-specific fine-tuning of host gene expression by SARS-CoV-2.

Baricitinib reversed IFN-induced gene expression changes (Fig. 4C). Genes that were highly induced upon IFN treatment were significantly down-regulated by baricitinib, including the IFN-stimulated genes (ISG) 15 and 20, chemokines (CCL8 and CXCL10), major histocompatibility complex components (CD74, LAG3, and LAMP3), and several members of the IFN-induced protein (IFIT) family. In contrast, baricitinib reverses the IFN-mediated inhibition of immunoreceptor signaling (SYK), metabolic remodelers (BCAT1 and KSR2), and transcriptional regulators (SOX4 and TLE2; Fig. 4, D and E). The only genes that escaped baricitinib action were serum amyloid A1 (SAA1) and its paralog SAA2, whose expression levels were decreased upon IFN treatment and even further reduced upon baricitinib.

Baricitinib binds to host NAKs

Ligand binding studies as carried out by Sorrell *et al.* (*30*) documented that all three of these closely related enzymes are effectively inhibited by baricitinib [BIKE K_d (dissociation constant) = 39.8 nM; AAK1 K_d = 17.2 nM; GAK K_d = 134.4 nM] (figs. S1 and S2). While the most relevant NAK in the inhibition of viral entry is unclear, BIKE (BMP-2-inducible protein kinase) was not expressed in liver cells, suggesting that AAK1 (AP2-associated protein kinase 1) and GAK (cyclin G-associated kinase) are sufficient to mediate viral entry. To disentangle the effects of baricitinib on replication and viral entry, we evaluated viral loads 4 hours after infection using baricitinib
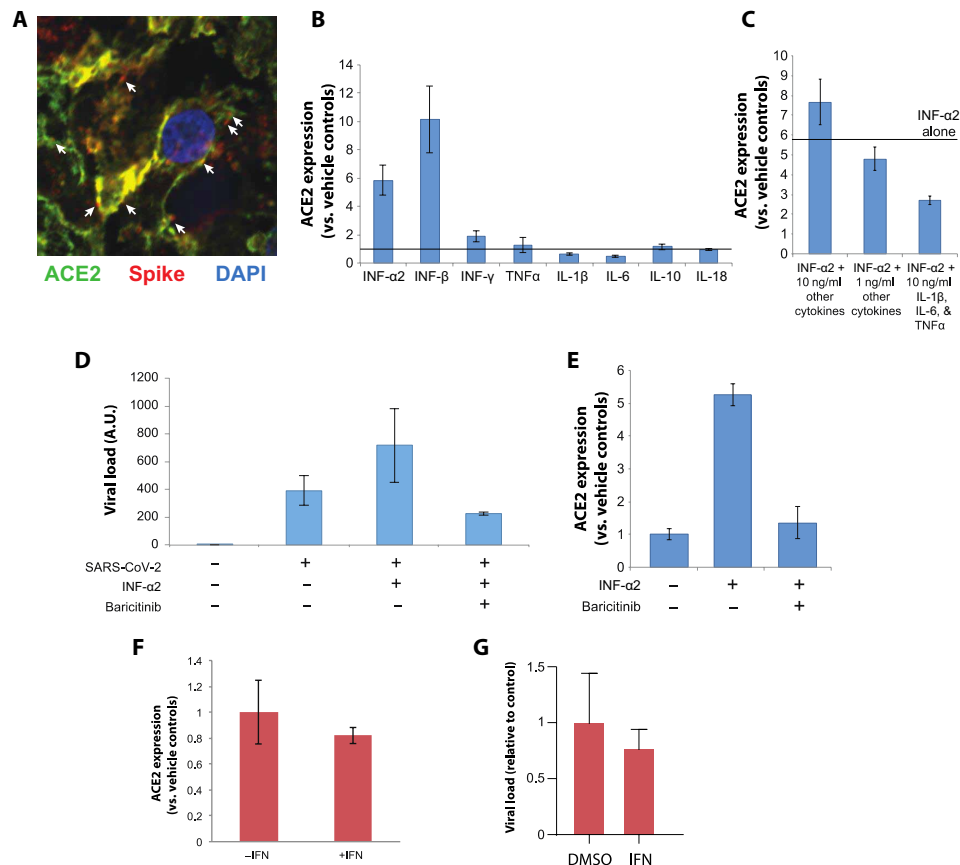
Fig. 3. Baricitinib inhibits cytokine-mediated increased infectivity of SARS-CoV-2 in organotypic primary human liver culture. (**A**) Immunofluorescence confocal imaging of a liver spheroid 48 hours after infection with SARS-CoV-2. Viral spike protein is shown in red, ACE2 in green, and DAPI (4′,6-diamidino-2-phenylindole) in blue. Arrows indicate examples of where spike protein and ACE2 signals are in close proximity. (**B**) Liver spheroids were treated with different cytokines (10 ng/ml), and the fold increase in ACE2 transcript levels are shown relative to controls (indicated by the solid line). Note that IFN-α2 and IFN-β significantly induce ACE2 levels. $N = 2$ technical replicates. (**C**) Combinatorial cytokine exposure does not result in increased ACE2 induction compared to IFN-α2 alone. "Other cytokines" corresponds to IFN-β, IFN-γ, TNFα, IL-1β, IL-6, IL-10, and IL-18. (**D**) IFN-α2 increases viral load in hepatocyte spheroids, and this effect is fully inhibited by baricitinib. $N = 2$ to 3 biological replicates. (**E**) IFN-α2–mediated induction of ACE2 is fully prevented by baricitinib. $N = 3$ biological replicates. All cytokine concentrations were 10 ng/ml unless stated otherwise. (**F**) ACE2 in lung organoids is not induced even by very high concentrations of IFN-α2 (50 ng/ml). $N = 3$ biological replicates. (**G**) By contrast, IFN-α2 slightly reduces viral load in lung organoids. $N = 3$ biological replicates. Error bars indicate SEM. A.U., arbitrary units; DMSO, dimethyl sulfoxide.

concentrations close to the relevant K_d values (100 nM). dSTORM superresolution microscopy revealed anti-nucleocapsid protein immunoreactivity clusters throughout the infected samples (Fig. 5A). In contrast, virus signals were almost absent in baricitinib-treated samples (Fig. 5B). The density of anti-nucleocapsid staining in baricitinib-treated spheroids was almost absent and in baricitinib-treated samples ($P < 0.001$) and reduced to levels found in noninfected controls, demonstrating that baricitinib efficiently blocked viral entry at nanomolar concentrations (Fig. 5C). These results were corroborated by quantitative polymerase chain reaction (qPCR) analyses, which showed significant reductions in intracellular viral loads, irrespective of IFN-mediated ACE2 induction (Fig. 5D). Combined, these data corroborate a dual-effect model for baricitinib in which the compound (i) inhibits the induction of IFN response genes, such as ACE2, resulting in reduced infectivity during the cytokine storm, and (ii) blocks viral entry by inhibition of NAKs (Fig. 5E).

Model building was also used to assess the potential impact of selected point mutations that occur with differing frequencies naturally, on baricitinib binding to BIKE (Ala[58]➔Asp, Ala[58]➔Val, Arg[134]➔Gln, Arg[134]➔Leu, Glu[131]➔Gln, Glu[131]➔Lys, and Ala[135]➔Thr), and mod-

eled baricitinib binding to both AAK1 (Ala[72]➔Thr and Gly[132]➔Val) and GAK (Glu[124]➔Val, Gly[128]➔Glu, and Gln[129]➔Arg). None of these point mutations appear likely to destabilize the structure of the kinase catalytic domain (i.e., disrupt packing in the hydrophobic core). In addition, none of these point mutations appear likely to disrupt baricitinib binding (table S1). All of the hydrogen bonds and van der Waals interactions observed between the drug and wild-type BIKE appear to be preserved for each point mutant (fig. S2A). The same holds true for the predicted hydrogen bonds and van der Waals interactions between the drug and mutant forms of AAK1 (fig. S2B) and the drug and mutant forms of GAK (fig. S2C), respectively.

DISCUSSION
Effective and well-tolerated treatments for patients infected with the novel coronavirus have proved elusive. Here, we link antiviral and anticytokine activities of baricitinib in hospitalized patients with COVID-19 pneumonia and in spheroid models of SARS-CoV-2 infection. During the pandemic's exponential phase, in investigator-led studies in both Italy and Spain, the treatment of hospitalized
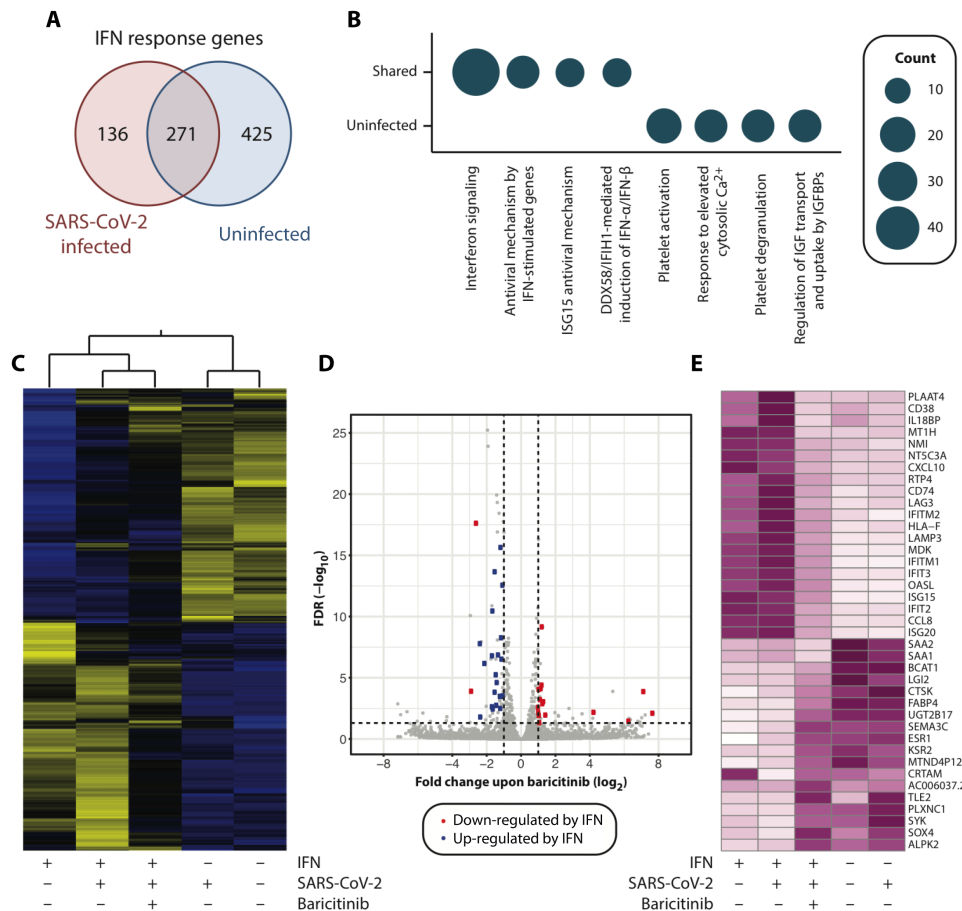
Fig. 4. Baricitinib reverses IFN-mediated gene expression signature alterations. (**A**) Venn diagram depicting the overlap of differentially expressed genes upon IFN-α2 (10 ng/ml) in SARS-CoV-2–infected and uninfected liver spheroids. (**B**) Circle plots illustrating significantly deregulated genes falling into specific Reactome terminologies in infected and noninfected samples (FDR < 0.05). Circle diameter is indicative for the number of genes per category. (**C**) Heatmap representation of IFN-responsive genes (*n* = 832). *z* scores of normalized TPMs (transcripts per million mapped reads) are plotted (purple, high; white, low). (**D**) Volcano plot showing the differentially expressed genes in all infected samples upon treatment with baricitinib. Blue and red dots indicate genes that are significantly up- and down-regulated upon IFN treatment. Note that with the exception of SAA1/2, baricitinib results in inverse changes to gene expression compared to IFN, thus ameliorating IFN-induced gene expression alterations. (**E**) Heatmap visualization of genes for which significant effects on gene expression were detected for baricitinib and IFN.

patients with COVID-19 using the JAK/STAT pathway inhibitor baricitinib has been associated with clinical improvement, findings that require assessment in randomized trials (*31*). The inclusion of a large cohort with a median age of 81 years merits particular attention here.

Baricitinib was generally well tolerated with a reduction in inflammation and substantially improved outcomes. In the matched populations, 16.9% of the baricitinib-treated patients died and/or progressed to invasive mechanical ventilation, compared to 34.9% in the standard-of-care group (*P* < 0.001; Fig. 2). Note that baricitinib's effects were evident from the first treatment days and maintained over follow-up (Fig. 2). Although most recommended treatment regimens support the use of 4 mg for 14 days, lower doses and shorter durations may be beneficial for certain populations including elderly patients described here. It is also remarkable from our data that in the propensity score–matched populations from both sites, most of the participants received similar treatment regimens with hydroxychloroquine, lopinavir/ritonavir, LMWH, and glucocorticoids. In Cox proportional hazard analyses, these treatments did not affect survival, while baricitinib was beneficial in univariate, multivariate, and time-related analyses (Table 4).

The main toxicities observed were hepatic, infectious, gastrointestinal, and cardiovascular, although in most cases, a definite causative relationship with baricitinib use could not be ascertained. An elevation in plasma transaminases occurred in some patients, and as previously observed, continuation of baricitinib was possible with resolution of liver function abnormalities. A recent case report in an 87-year-old severely unwell patient from Foggia, Italy showed that its use was associated with rapid clinical improvement in stark contrast to her infected husband and son who did not receive baricitinib and died (*32*). While these reports are inconclusive, in aggregate, these data strongly support the continued investigation of baricitinib for COVID-19 in ongoing randomized control trials, including ACTT-II (NCT04401579), where baricitinib is given in combination with remdesivir, TACTIC-R (NCT04390464), and others including NCT04373044. Multivariate analyses that we performed showed no differences in corticosteroid type (prednisolone, dexamethasone, hydrocortisone, or methylprednisolone), duration, dose, and outcome.

Age appears the most relevant risk factor for adverse outcomes related to COVID-19 (*16*). In patients with COVID-19 pneumonia, immune dysfunction is present, even in mild cases (*25*), and immune
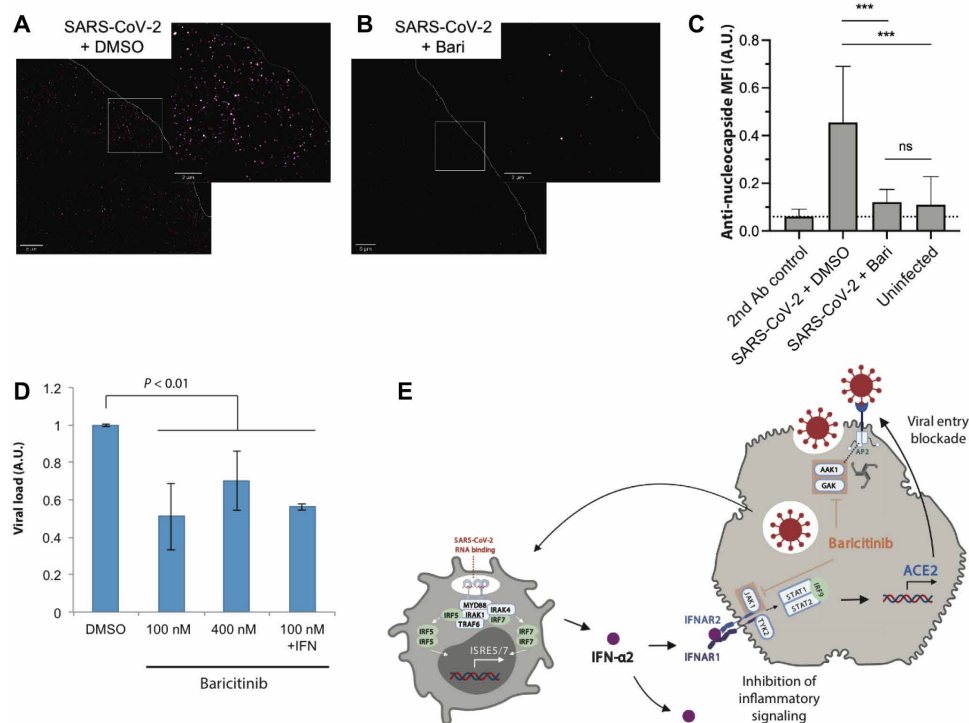
Fig. 5. Baricitinib blocks viral entry of SARS-CoV-2. Superresolution dSTORM microscopy of short-term (4 hours) infected liver spheroids stained for nucleocapsid treated with vehicle control (**A**) or baricitinib (100 nM) (**B**). (**C**) Relative mean fluorescence intensities (MFIs) for regions with dimensions of 20 μm by 20 μm of infected and treated organoids and secondary antibody–only controls; five regions per 3D tissue culture. Bars are means ± SD; ***$P < 0.001$ two-tailed Student's t test. Ab, antibody; ns, not significant. (**D**) qPCR analysis of viral load in organotypic primary human liver culture following short-term (4 hours) infections corroborates inhibition of viral entry. (**E**) Suggested mechanism of dual baricitinib antiviral action on viral entry and inflammatory signaling. Baricitinib inhibits on viral entry by inhibition of the NAKs AAK1 and GAK. In addition, baricitinib blocks inflammatory JAK/STAT signaling, resulting in reduced expression of the IFN target gene and SARS-CoV-2 receptor ACE2. A plasmacytoid dendritic cell is shown on the left, and a hepatocyte is shown on the right.

responses in older adults are slower, less coordinated, and less efficient, so-called immunosenescence (*33*). Until now, there have been no clinical trials or post-authorization studies that have demonstrated efficacy or safety of commonly used drugs in much older adults hospitalized with COVID-19, an especially vulnerable and susceptible population, and age is often an exclusion criterion in trials, as is frailty.

One concern in early disease is amelioration of the antiviral activity of type-1 IFNs, which signal through JAK/STAT pathways. Our study using viral infection assays in liver spheroids confirms that ACE2 is an ISG, supporting previous data (*34*). This induction should increase viral infectivity rather than reduce it. This was observed in human hepatocytes, which normally express low levels of this receptor, in contrast to endothelial cells where ACE2 is abundantly expressed and contributes to the local control of perfusion. This, in turn, suggests that extrapulmonary effects of COVID-19 may be mediated by type-1 IFN–mediated increases in ACE2 expression, both on endothelial and parenchymal cells, resulting in endotheliitis (*24*) and liver injury in up to 60% of severely ill patients (*35*). While deficiency in type-1 IFN immunity is associated with life-threatening COVID-19 pneumonia (*36*), induction of IFNs and ISGs is detected in some critically ill patients (*37*). In aggregate with our findings in liver spheroids, these data suggest that type I IFNs play an important bivalent role in COVID pathobiology that requires tight regulation and lead us to hypothesize that JAK/STAT inhibitors could be beneficial early in the course of the disease by reducing IFN-I–induced ACE2 expression. Notably, we found important qualitative differences

between the response of liver spheroids, where IFNs induced ACE2 and increased infectivity, and lung organoids, where ACE2 and viral load were not affected by IFN signaling. Vascular endothelial cells express high levels of ACE2 (*38*); however, while endothelial cells are highly responsive to IFN signaling (*39*), whether ACE2 constitutes an IFN response gene remains to be elucidated. Combined, these data suggest that the effects of baricitinib might differ between organ systems, and we could speculate that the anti-inflammatory effects might be most beneficial in those tissues in which ACE2 is an IFN response gene, including liver. It will be interesting to see whether further systematic analyses of the effect of IFNs on ACE2 expression and infectivity across human tissues will confirm these hypotheses.

To further validate our data in early patients and strengthen the safety database, we also present results for an additional 48 patients with mild-moderate pneumonia treated at two hospitals in Italy (Table 5 and table S1); a transient transaminitis was observed in two individuals, and all patients recovered uneventfully, with the most common drug-induced adverse event in 131 baricitinib-treated individuals presented here.

The susceptibility of liver spheroids to SARS-CoV-2 infection was, at first, unexpected to us but ties in with the transaminitis observed. Note that SARS-CoV-2 can productively infect human gut enterocytes, as shown using human small intestinal organoids (*40*). We have analyzed ACE2 expression in available proteomics and RNA-seq data and detected low-level ACE2 transcripts or protein with average FPKM (fragments per kilobase of transcript per million mapped reads) data across three donors of 0.95 (*41*). These levels are consistent

Table 5. Baseline demographic, clinical, and laboratory characteristics of patients with COVID-19 treated with either baricitinib or with standard COVID-19 therapy and results at 2 weeks from the Hospital of Prato. Standard univariate statistical tests were performed to compare baricitinib-treated patients to age- and sex-matched controls. These consisted of the Mann-Whitney U test for pairwise comparisons, the Wilcoxon test for paired data, and Fisher's exact test for categorical variables. Kaplan-Meier product-limit estimation and the log-rank test were used to perform a survival analysis between groups. A dose of 4 mg daily of baricitinib was given for 14 days. SpO_2, peripheral capillary oxygen saturation; SBP, systolic blood pressure; DBP, diastolic blood pressure; WBC, white blood cells; MEWS, modified early warning score; CVD, cardiovascular disease; NA, not applicable; IQR, interquartile range; ICU, intensive care unit.

Features at baseline (all patients received hydroxychloroquine and lopinavir/ritonavir)	Baricitinib group	Control group*	P value
Patient number, N (%)	23 (100)	18 (100)	
Male/female, N (%)	20/3 (87/13)	14/4 (78/22)	0.679
Age years, median (IQR)	62.5 (57.75–72.25)	64.1 (55.7–70.1)	0.776
Days interval from symptoms onset and therapy starting	6 (4–6.25)	5.5 (4–5.25)	0.924
Cough, N (%)	17 (73.9)	15 (83.3)	0.709
Dyspnea, N (%)	20 (86.9)	14 (77.8)	0.679
Sputum production, N (%)	7(30.4)	9 (50)	0.334
Headache, N (%)	8 (34.8)	7 (38.9)	0.757
Diarrhea, N (%)	5 (21.7)	5 (27.8)	0.524
Ageusia/anosmia, N (%)	9 (39.1)	8 (44.4)	0.860
Hypertension, N (%)	5 (21.7)	6 (33.3)	0.489
Diabetes, N (%)	6 (26)	4 (22.2)	1.000
COPD, N (%)	5 (21.7)	4 (22.2)	1.000
CVD, N (%)	4 (17.4)	2 /11.1)	0.679
Malignancy, N (%)	1 (4.3)	1 (5.5)	1.000
Fever (°C)	38 (37.5–38.6)	37.9 (37.6–38.9)	0.912
Respiratory rate (N/min)	18 (16.5–23.2)	21 (18–24)	0.524
SpO_2 (%)	94 (90–95.5)	92 (91–93)	0.357
PaO_2/FiO_2, median (IQR)	293 (199–296)	271.4 (264–283)	0.356
Pulse rate, median (IQR)	84 (72.3–89.1)	88 (86–94.5)	0.129
SBP mm/Hg, median (IQR)	110 (100–130)	105 (98–115.6)	0.789
DBP mm/Hg, median (IQR)	70 (60–84)	65.5 (60–68.5)	0.589
WBC ($\times10^9$/liter), median (IQR)	7.6 (5.7–10.4)	7.9 (7.1–8.6)	0.757
Neutrophils ($\times10^9$/liter), median (IQR)	6,3 (4.2–7.8)	7.1 (6.4–8.1)	0.224
Lymphocytes ($\times10^9$/liter), median (IQR)	0.6 (0.5–1.1)	0.72 (0.6–0.8)	0.524
Hemoglobin (g/liter), median (IQR)	116 (102–133.2)	127 (108–136)	0.565
Platelets ($\times10^9$/liter), median (IQR)	207 (174–232)	368 (340–415)	0.002
ALT (IU/liter), median (IQR)†	27.6 (22.7–53.1)	44 (36–50)	0.176
AST (IU/liter), median (IQR)	31 (25.2–47.3)	44 (34.7–48)	0.235
ALT (IU/liter) > upper normal limit N (%)	8 (34.7)	9 (50)	0.358
ALT (IU/liter) > upper normal limit, median (IQR)	50 (45.5–62.7)	55 (45–68)	0.707
AST (IU/liter) > upper normal limit N/%	10	11	0.350
AST (IU/liter) > upper normal limit, median (IQR)	51.5 (44.5–76.5)	67 (55–80)	0.302
Creatinine (mg/dl), median (IQR)	1.0 (0.9–1.3)	1.1 (0.9–1.2)	0.789
CRP (mg/dl), median (IQR)	9.12 (5.9–16.5)	4.3 (1.5–5.2)	0.001
Procalcitonin (ng/ml), median (IQR)	0.5 (0.3–1.0)	1.1 (0.8–2.2)	0.589
IL-6 (pg/ml)‡, median (IQR)	29.2 (7.1–39.4)	24.2 (5.2–27.6)	0.189

Continued on the next page

Features at baseline (all patients received hydroxychloroquine and lopinavir/ritonavir)	Baricitinib group	Control group*	P value
MEWS, median (IQR)	2 (1–3.1)	3 (3–4)	0.544
Results at 2 weeks after therapy			
ICU admission N (%)	0	5 (33)	0.011
Discharged, N (%)	18 (78.2)	1 (5.5)	<0.0001
SpO$_2$, median (IQR)	97 (94.8–98.1)	92.4 (85.5–93.2)	<0.0001
PaO$_2$/FiO$_2$ value, median (IQR)	428.7 (306.1–457)	277.8 (144–345)	0.002
Lymphocytes (×10^9/liter), median (IQR)	1.3 (1.2–1.9)	0.8 (0.6–0.9)	0.019
CRP (mg/dl), median (IQR)	0.87 (0.58–2.9)	5.2 (2.1–12.3)	<0.0001
IL-6 (pg/ml)‡, median (IQR)	6.1 (3.2–7.4)	NA	NA
ALT (IU/liter), median (IQR)	37 (24.1–57.4)	NA	NA
AST (IU/liter), median (IQR)	55.4 (28–64.3)	NA	NA

*Standard therapy group: Patients with COVID-19 under standard respiratory therapy commenced antiretrovirals (Kaletra) and hydroxychloroquine before starting the therapy with baricitinib.   †Normal ALT and AST values: 10 to 40 IU/liter.   ‡IL-6 normal value: <7 pg/ml.

with previous data indicating low but detectable levels of ACE2 in liver cells (*42*). We have also interrogated the The Cancer Genome Atlas with the UALCAN database and found low levels of ACE2 transcripts in peritumoral liver cells in hepatocellular carcinoma data.

The demonstration that baricitinib inhibited viral infectivity in vitro, as well as having an overall anti-inflammatory effect in vivo, confirms predictions arising from the use of AI and the comprehensive biomedical knowledge graph (*7–9*). It also demonstrates that compiling such an AI-enriched database, with its associated algorithms, enables the identification of relationships, in this case, the ability of a single approved drug to both inhibit viral infectivity and ameliorate the exuberant inflammatory consequences of viral infection. It also enables network effects to be identified quickly, which is of enormous importance when trying to identify therapeutics in the midst of a global pandemic (*10*).

We did not observe any thrombotic or vascular events in our cohort, a previously raised possible concern with the use of baricitinib and also an increasing concern in general with COVID-19 infection (*14, 43, 44*), although most patients (86%) here received LMWH. The short half-life of baricitinib ($t_{1/2}$ = 12.5 hours) versus the anti–IL-6 antibodies such as tocilizumab (t = 13 days), oral once/daily administration, and lack of drug-drug interactions (it is excreted largely unchanged), we believe, lend itself to use during a short-term viral infection and also the possibility of utility in low- and middle-income countries. A glomerular filtration rate (GFR) of <30 ml/min is a limitation for the higher 4-mg dose, but a 2-mg dose can be used: We highlight from the Spanish cohort that specifically shows that baricitinib may be safe and effective with the lower 2-mg dose and fewer treatment days. Randomized trials are needed in this elderly population, and note, for example, that many other studies (e.g., for remdesivir) exclude elderly individuals or those with a GFR of <50 ml/min. Other features such as its potential to cross the blood-brain barrier and help ameliorate neurologic sequelae may also be beneficial in selected patients, as we have described (*45, 46*). Trials of other JAK inhibitors such as ruxolitinib are ongoing, and the same principles may apply (*47*), although our knowledge graph specifically called out baricitinib among these related molecules (*9*). We noted that the brain:plasma ratio for baricitinib measured 5× that for ruxolitinib (*45*). Furthermore, the computational docking results (figs. S3

and S4) suggest that any one or two or all three of the NAKs could be the baricitinib target(s) relevant to our clinical findings, although BIKE is unexpressed on liver spheroids so the target is likely to be AAK1 and/or GAK. We consider it unlikely that baricitinib is acting on an alternative protein target(s) that may not even be a protein kinase, but we cannot rule out this possibility. For example, TMPRSS2, a membrane-bound serine protease that primes the spike protein (*48*), is also well known to be important for viral entry via ACE2. IL-6 signaling (*49*) is related to its expression, and baricitinib, which reduces IL-6 levels in a dose-dependent manner, may affect its expression. Should additional clinical studies confirm the benefits of baricitinib in managing advanced SARS-CoV-2 infections, efforts aimed at identification of the precise molecular target(s) would be useful here.

Notwithstanding our findings supporting the hypothesis that baricitinib is clinically active and safe in this setting, there are several limitations in our study that need to be acknowledged. This was not a randomized trial comparing baricitinib to a placebo control group. Therefore, known and unknown confounding variables could have compromised the results. The propensity score–matching procedure eliminated much of the group imbalance in known confounding variables, but some imbalance remained in important parameters such as existing comorbidities. In addition, the sample size from the final baricitinib cohort was small, limiting overall statistical power. Multiple statistical tests were performed without an adjustment for multiplicity, which increases the risk of a type I statistical error. Given these limitations, we eagerly await the completion of the baricitinib randomized trials that are currently ongoing.

In summary, we have confirmed dual actions of baricitinib, demonstrating its ability to inhibit viral entry into primary human hepatocyte spheroids and the reduction in inflammatory markers in patients with COVID-19 as per our suggested model (Fig. 5C). In addition, we show that baricitinib prevents the type-1 IFN–mediated increase in expression of ACE2, the receptor for SARS-CoV-2.

METHODS
Patients and statistics
Two observational studies from Italy and Spain were conducted, approved by the Internal Review Boards (IRBs) of each institution.

Entry criteria for each institution included patients with radiologically defined COVID-19 pneumonia and laboratory-confirmed infection, as diagnosed by a positive SARS-CoV-2 RT-PCR (reverse transcription PCR) test by nasopharyngeal swab. All patients enrolled had a blood oxygen saturation (SaO$_2$) < 94% at baseline but did not require mechanical ventilation. The Pisa, Italy cohort included all consecutive cases with SARS-CoV-2 pneumonia and PaO$_2$/FiO$_2$ (P/F) ratio of <300 mmHg at admission diagnosed between the period of 7 and 31 March 2020 and had moderate-to-severe or severe disease. The COVID-AGE study from Albacete, Spain (NCT04362943) was conducted at Complejo Hospitalario Universitario of Albacete, dedicated to older adults; thus, baricitinib doses were lower than in Italy. The Albacete cohort included patients ≥70 years with SARS-CoV-2 pneumonia, diagnosed between 9 March and 20 April 2020, not requiring mechanical ventilation, and again having moderate-to-severe or severe disease.

Written informed consent was obtained from each patient in Italy and verbal informed consent in Spain as approved by the local IRB. Baricitinib was administered at a dose of 4 mg/day for 14 days in conjunction with standard of care in Italy and at lower doses of 2 or 4 mg/day for 3 to 11 days in the Spanish cohort because of age-related factors. Any patient with confirmed COVID-19 infection who received at least three doses of baricitinib was included in the intent-to-treat analysis. Standard clinical and laboratory data were collected including patients' demographics, comorbidities, oxygen support, adverse events, laboratory values, concomitant therapies, and clinical outcomes. Exclusion criteria in all patients included a history of active or latent tuberculosis infection (QuantiFERON Plus-test positivity, QIAGEN, Germany), pregnancy, and/or lactation. The primary outcome was death from any cause or intensive care unit admission needing invasive mechanical ventilation during hospitalization.

For both cohorts, propensity score matching was used to create the control selection sample using patients admitted in the same period of time in both hospitals, not treated with baricitinib. Cases and controls were matched for relevant predictors of respiratory failure and death, as well as baseline treatments. The following variables, all of them clinically relevant for mortality and respiratory failure, were included in the propensity score estimation: age, sex, chronic obstructive pulmonary disease, arterial hypertension, cardiovascular disease, diabetes mellitus, chronic kidney failure, Charlson comorbidity index, baseline P/F ratio, lymphocyte count, therapy with steroids, LMWH, and "antiviral" therapy with hydroxychloroquine or protease inhibitors (lopinavir/ritonavir). Propensity score matching was conducted with the statistical package MatchIt (v4.0.2), using the recommendations from Ho et al. (50) to improve parametric models and preprocessing of nonparametric data. After the propensity score was determined for each patient, those treated with baricitinib were matched to 1:1 to a control patient using a greedy matching procedure with replacement, targeting the average treatment effect on the treated replacement. Continuous variables were tested using Wilcoxon-Mann-Whitney rank sum test; categorical variables were tested using Pearson's chi-square or Fisher's exact test. For every test performed, the P value was always above 0.05, and therefore, we can say that the groups were homogeneous regarding the control variables. Validity of the balance in potential confounding variables was assessed visually with normality plots using the "R" function ["geom:smooth()" using formula "y ~ x"], also using the Wilcoxon rank sum test with continuity correction analyses for continuous variables, and with Pearson's chi-square tests for categorical ones.

Although the matching figures were not perfect, no statistical differences were found for any variables included in the propensity score in the merged Pisa and Albacete cohorts. Mortality reduction was analyzed with Cox proportional hazard models adjusted for all the variables included in the propensity score matching, to further control for the small deviations in the matching procedure, plus the presence of active cancer, alanine aminotransferase, and antibiotic use. Safety data are presented in a descriptive manner. Last, individual and merged data from Pisa and Albacete were used to analyze the primary outcome, survival, or mechanical ventilation, in baricitinib and control groups using Kaplan-Meier analysis, including 95% CIs. The global significance was determined using a Peto-Peto analysis that prioritizes the first part of the curves but with increased robustness compared to Taron-Ware analysis. This decision was taken after the observation that the main differences between baricitinib and control patients were present from the beginning of the treatment. Statistical significance was established at $P < 0.05$ using a two-sided test statistic. All analyses were done using the statistical package R.

Human spheroid and organoid culture, cytokine exposures, and SARS-CoV-2 infections

SARS-CoV-2 (GenBank accession number MT093571) was isolated from a nasopharyngeal sample of a patient in Sweden on Vero E6 cells. Organotypic 3D primary human liver cultures with physiological transcriptomic, proteomic, and metabolomic profiles were cultured as previously described (51–53). In short, cryopreserved primary human hepatocyte (BioIVT, USA) were thawed, and the isolated cell suspensions were seeded into 96-well ultralow attachment plates (Corning) with 1500 cells per well. In short, cells were seeded in 100 µl of Williams E medium supplemented with 2 mM L-glutamine, penicillin (100 U/ml), streptomycin (100 µg/ml), insulin (10 µg/ml), transferrin (5.5 µg/ml), sodium selenite (6.7 ng/ml), 100 nM dexamethasone, and 10% fetal bovine serum. Spontaneous self-aggregation of the hepatocytes occurred, and after few days, a single spheroid could be observed per well. Once spheroids were sufficiently compact (after day 5), cell aggregates were preexposed to baricitinib and/or cytokines.

Formed liver spheroids and pulmonary organoids were exposed for 1 day with reconstituted human IFN-α2 (BioLegend, no. 592706), IFN-β (R&D Systems, no. 8499-IF-010), IFN-γ (BioLegend, no. 570206), IL-1β (BioLegend, no. 579406), IL-6 (R&D Systems, no. 206-IL-050), IL-10 (R&D Systems, no. 217-IL-010), IL-18 (BioLegend, no. 592104), and TNFα (R&D Systems, no. 210-TA-100) either alone or in combination with baricitinib before viral infections. Cytokine concentrations were 10 ng/ml unless stated otherwise. Following these preexposures, cells were infected with SARS-CoV-2 at a multiplicity of infection of 0.1 in triplicate for 48 hours. After 48 hours, spheroids were washed with phosphate-buffered saline (PBS), pooled (32 wells per condition), and lysed using TRIzol (Thermo Fisher Scientific). RNA was extracted using Direct-zol mini kit (Zymo Research), and relative levels of ACE2 and viral RNA were determined by qRT-PCR as described (54).

Confocal microscopy

Primary human hepatocyte spheroids were fixed in 4% paraformaldehyde for at least 4 hours and washed with PBS. For cryoprotection, spheroids were incubated with 30% sucrose in PBS at 4°C overnight or until the microtissues sank. Subsequently, they were washed with PBS

and transferred into micromolds for OCT (optimal cutting temperature) cryo-mount embedding. OCT-embedded spheroids were frozen in an isopropanol dry ice bath and were sectioned at 8-μm thickness on a CryoStar NX70 cryostat. Sections were washed twice with PBS for 10 min and blocked with PBTA buffer [5% bovine serum albumin (BSA), 0.25% Triton X-100, and 0.01% NaN₃ in PBS] for 2 hours at room temperature. Subsequently, the blocked sections were incubated overnight at 4°C with the monoclonal primary antibody anti-1A9 (diluted in PBTA to a final concentration of 5 μg/ml). Samples were washed 3 × 15 min with PBS at room temperature before incubation with the secondary antibody (donkey anti-mouse diluted in PBTA at 1:500) for 2 hours at room temperature. Unbound secondary antibody was washed out three times with PBS (15 min each) at room temperature, and the slides were mounted with 4′,6-diamidino-2-phenylindole Gold Antifade.

Superresolution microscopy

Sections, prepared as above, were thawed and rehydrated using PBS then blocked for 30 min using a blocking buffer containing 10% goat serum, 2% BSA, and 0.3% Triton X-100. Primary antibody against nucleocapsid was diluted at 1:500 in 10% goat serum and 2% BSA and incubated overnight at 4°C. Sections were then washed with PBS 3 × 10 min. Primary antibodies were detected with Alexa Fluor 647–conjugated secondary goat anti-mouse F(ab′)2 (Abcam, ab98758) diluted to 500 ng/ml in 10% goat serum and 2% BSA for 1 hour at room temperature. Last, sections were washed 5 × 10 min and mounted using an ONI B-Cubed imaging buffer. Superresolution images were acquired on the Nanoimager S Mark II from ONI (Oxford Nanoimaging) equipped with 405-nm/150-mW, 473-nm/1-W, 560-nm/1-W, and 640-nm/1-W lasers and dual emission channels split at 640 nm. To achieve single-molecule blinking, samples were irradiated with the 640-nm laser, and then, 10,000 frames were acquired in an appropriate focal plane at 30 Hz. Single-molecule data were filtered on the basis of photon count, precision, and sigma value in NimOS. All samples were filtered using the same parameters.

RNA sequencing

RNA was isolated from 3D liver tissue samples and were ribosomal RNA (rRNA) depleted, followed by strand-specific RNA library generation (Takara SMART-Seq Stranded kit). RNA libraries were sequenced paired end (75 + 75 cycles) on an Illumina NextSeq 500 device. On average, 20 million reads per sample were obtained, low-quality reads were removed, and ends were trimmed using Trimmomatic (version 0.36). rRNA contamination was determined by mapping to a customized human rRNA reference genome (HISAT2 version 2.1.0). Approximately, 8 to 15% rRNA contamination was found in the samples, which is below the manufacturer's expected range between 15 and 35%. Nonaligned reads were further mapped to the human reference genome (downloaded from University of California, Santa Cruz, hg38). After mapping to the human genome, generated .bam files were processed using samtools (version 1.10). Bedgraph files were generated using Homer (version 4.11). Last, count tables were generated using the tool Subread (version 2.0.0).

Differential gene expression analysis was performed using both DESeq2 (version 1.26) and edgeR (version 3.28). For both methods, genes with zero counts were filtered out, and more than eight counts in at least 2 of the 12 samples were considered further. In DESeq2, independent filtering and Cook's distance were set to false. In edgeR, the glmLRT method was used. Only genes with log₂ FC > |1| and

FDR < 0.05 were considered. When intersecting the number of differentially expressed genes identified using the two methods, we found an overlap of >90% and continued the analysis by using the data obtained from DESeq2. Pathway analysis was performed using the R package ReactomePA (version 1.30.0).

Computational structure analysis

3D atomic-level structures of NAKs BIKE [Protein Data Bank (PDB) ID 4w9x], AAK1 (PDB ID 4wsq), and GAK (PDB ID 4y8d) were compared at the level of amino acid sequence and 3D structure (figs. S1 and S2). Superposition computational docking using the experimental structure of the BIKE-baricitinib protein:drug complex (PDB ID 4w9x) was used to investigate the modes of binding of baricitinib to both AAK1 and GAK (fig. S2). Figures were generated using UCSF Chimera (55).

REFERENCES AND NOTES

1. A. S. Fauci, H. C. Lane, R. R. Redfield, Covid-19—Navigating the uncharted. *N. Engl. J. Med.* **382**, 1268–1269 (2020).
2. C. I. Paules, H. D. Marston, A. S. Fauci, Coronavirus infections—More than just the common cold. *JAMA* **323**, 707–708 (2020).
3. Z. Wu, J. M. McGoogan, Characteristics of and important lessons from the coronavirus disease 2019 (COVID-19) outbreak in China: Summary of a report of 72314 cases from the Chinese Center for Disease Control and Prevention. *JAMA* **323**, 1239–1242 (2020).
4. Y. Tanaka, K. Emoto, Z. Cai, T. Aoki, D. Schlichting, T. Rooney, W. Macias, Efficacy and safety of baricitinib in Japanese patients with active rheumatoid arthritis receiving background methotrexate therapy: A 12-week, double-blind, randomized placebo-controlled study. *J. Rheumatol.* **43**, 504–511 (2016).
5. L. R. Baden, E. J. Rubin, Covid-19 - The search for effective therapy. *N. Engl. J. Med.* **382**, 1851–1852 (2020).
6. A. Mullard, COVID-19 vaccine development pipeline gears up. *Lancet* **395**, 1751–1752 (2020).
7. P. Richardson, I. Griffin, C. Tucker, D. Smith, O. Oechsle, A. Phelan, M. Rawling, E. Savory, J. Stebbing, Baricitinib as potential treatment for 2019-nCoV acute respiratory disease. *Lancet* **395**, e30–e31 (2020).
8. P. J. Richardson, M. Corbellino, J. Stebbing, Baricitinib for COVID-19: A suitable treatment?—Authors' reply. *Lancet Infect. Dis.* **20**, 1013–1014 (2020).
9. J. Stebbing, V. Krishnan, S. de Bono, S. Ottaviani, G. Casalini, P. J. Richardson, V. Monteil, V. M. Lauschke, A. Mirazimi, S. Youhanna, Y.-J. Tan, F. Baldanti, A. Sarasini, J. A. R. Terres, B. J. Nickoloff, R. E. Higgs, G. Rocha, N. L. Byers, D. E. Schlichting, A. Nirula, A. Cardoso, M. Corbellino; Sacco Baricitinib Study Group, Mechanism of baricitinib supports artificial intelligence-predicted testing in COVID-19 patients. *EMBO Mol. Med.* **12**, e12697 (2020).
10. M. B. Schultz, V. Vera, D. A. Sinclair, Can artificial intelligence identify effective COVID-19 therapies? *EMBO Mol. Med.* **12**, e12817 (2020).
11. B. K. Titanji, M. M. Farley, R. Connor-Schuler, A. Mehta, R. Moanna, S. K. Cribbs, J. O'Shea, K. De Silva, B. Chan, A. Edwards, C. Gavegnano, R. F. Schinazi, V. C. Marconi, Use of baricitinib in patients with moderate and severe COVID-19. *Clin. Infect. Dis.* **2020**, ciaa879 (2020).
12. J. S. Fridman, P. A. Scherle, R. Collins, T. C. Burn, Y. Li, J. Li, M. B. Covington, B. Thomas, P. Collier, M. F. Favata, X. Wen, J. Shi, R. M. Gee, P. J. Haley, S. Shepard, J. D. Rodgers, S. Yeleswaram, G. Hollis, R. C. Newton, B. Metcalf, S. M. Friedman, K. Vaddi, Selective inhibition of JAK1 and JAK2 is efficacious in rodent models of arthritis: preclinical characterization of INCB028050. *J. Immunol.* **184**, 5298–5307 (2010).
13. M. C. Genovese, J. Kremer, O. Zamani, C. Ludivico, M. Krogulec, L. Xie, S. D. Beattie, A. E. Koch, T. E. Cardillo, T. P. Rooney, W. L. Macias, S. de Bono, D. E. Schlichting, J. S. Smolen, Baricitinib in patients with refractory rheumatoid arthritis. *N. Engl. J. Med.* **374**, 1243–1252 (2016).
14. P. C. Taylor, E. C. Keystone, D. van der Heijde, M. E. Weinblatt, L. Del Carmen Morales, J. R. Gonzaga, S. Yakushin, T. Ishii, K. Emoto, S. Beattie, V. Arora, C. Gaich, T. Rooney, D. Schlichting, W. L. Macias, S. de Bono, P. Tanaka, Baricitinib versus placebo or adalimumab in rheumatoid arthritis. *N. Engl. J. Med.* **376**, 652–662 (2017).
15. C. Huang, Y. Wang, X. Li, L. Ren, J. Zhao, Y. Hu, L. Zhang, G. Fan, J. Xu, X. Gu, Z. Cheng, T. Yu, J. Xia, Y. Wei, W. Wu, X. Xie, W. Yin, H. Li, M. Liu, Y. Xiao, H. Gao, L. Guo, J. Xie,

G. Wang, R. Jiang, Z. Gao, Q. Jin, J. Wang, B. Cao, Clinical features of patients infected with 2019 novel coronavirus in Wuhan, China. *Lancet* **395**, 497–506 (2020).

16. F. Zhou, T. Yu, R. Du, G. Fan, Y. Liu, Z. Liu, J. Xiang, Y. Wang, B. Song, X. Gu, L. Guan, Y. Wei, H. Li, X. Wu, J. Xu, S. Tu, Y. Zhang, H. Chen, B. Cao, Clinical course and risk factors for mortality of adult inpatients with COVID-19 in Wuhan, China: A retrospective cohort study. *Lancet* **395**, 1054–1062 (2020).

17. M. Ackermann, S. E. Verleden, M. Kuehnel, A. Haverich, T. Welte, F. Laenger, A. Vanstapel, C. Werlein, H. Stark, A. Tzankov, W. W. Li, V. W. Li, S. J. Mentzer, D. Jonigk, Pulmonary vascular endothelialitis, thrombosis, and angiogenesis in Covid-19. *N. Engl. J. Med.* **383**, 120–128 (2020).

18. O. Gross, O. Moerer, M. Weber, T. B. Huber, S. Scheithauer, COVID-19-associated nephritis: Early warning for disease severity and complications? *Lancet* **395**, e87–e88 (2020).

19. F. Liu, L. Li, M. D. Xu, J. Wu, D. Luo, Y. S. Zhu, B. X. Li, X. Y. Song, X. Zhou, Prognostic value of interleukin-6, C-reactive protein, and procalcitonin in patients with COVID-19. *J. Clin. Virol.* **127**, 104370 (2020).

20. Q. Ruan, K. Yang, W. Wang, L. Jiang, J. Song, Clinical predictors of mortality due to COVID-19 based on an analysis of data of 150 patients from Wuhan, China. *Intensive Care Med.* **46**, 846–848 (2020).

21. J. Stebbing, A. Phelan, I. Griffin, C. Tucker, O. Oechsle, D. Smith, P. Richardson, COVID-19: Combining antiviral and anti-inflammatory treatments. *Lancet Infect. Dis.* **20**, 400–402 (2020).

22. Y. Wang, D. Zhang, G. Du, R. Du, J. Zhao, Y. Jin, S. Fu, L. Gao, Z. Cheng, Q. Lu, Y. Hu, G. Luo, K. Wang, Y. Lu, H. Li, S. Wang, S. Ruan, C. Yang, C. Mei, Y. Wang, D. Ding, F. Wu, X. Tang, X. Ye, Y. Ye, B. Liu, J. Yang, W. Yin, A. Wang, G. Fan, F. Zhou, Z. Liu, X. Gu, J. Xu, L. Shang, Y. Zhang, L. Cao, T. Guo, Y. Wan, H. Qin, Y. Jiang, T. Jaki, F. G. Hayden, P. W. Horby, B. Cao, C. Wang, Remdesivir in adults with severe COVID-19: A randomised, double-blind, placebo-controlled, multicentre trial. *Lancet* **395**, 1569–1578 (2020).

23. RECOVERY Collaborative Group, P. Horby, W. S. Lim, J. R. Emberson, M. Mafham, J. L. Bell, L. Linsell, N. Staplin, C. Brightling, A. Ustianowski, E. Elmahi, B. Prudon, C. Green, T. Felton, D. Chadwick, K. Rege, C. Fegan, L. C. Chappell, S. N. Faust, T. Jaki, K. Jeffery, A. Montgomery, K. Rowan, E. Juszczak, J. K. Baillie, R. Haynes, M. J. Landray, Dexamethasone in hospitalized patients with Covid-19—Preliminary report. *N. Engl. J. Med.* , (2020).

24. Z. Varga, A. J. Flammer, P. Steiger, M. Haberecker, R. Andermatt, A. S. Zinkernagel, M. R. Mehra, R. A. Schuepbach, F. Ruschitzka, H. Moch, Endothelial cell infection and endotheliitis in COVID-19. *Lancet* **395**, 1417–1418 (2020).

25. W. Li, M. J. Moore, N. Vasilieva, J. Sui, S. K. Wong, M. A. Berne, M. Somasundaran, J. L. Sullivan, K. Luzuriaga, T. C. Greenough, H. Choe, M. Farzan, Angiotensin-converting enzyme 2 is a functional receptor for the SARS coronavirus. *Nature* **426**, 450–454 (2003).

26. J. Shang, Y. Ye, K. Shi, Y. Wan, C. Luo, H. Aihara, Q. Geng, A. Auerbach, F. Li, Structural basis of receptor recognition by SARS-CoV-2. *Nature* **581**, 221–224 (2020).

27. A. J. Wilk, A. Rustagi, N. Q. Zhao, J. Roque, G. J. Martínez-Colón, J. L. M. Kechnie, G. T. Ivison, T. Ranganath, R. Vergara, T. Hollis, L. J. Simpson, P. Grant, A. Subramanian, A. J. Rogers, C. A. Blish, A single-cell atlas of the peripheral immune response in patients with severe COVID-19. *Nat. Med.* **26**, 1070–1076 (2020).

28. K.-J. Huang, I.-J. Su, M. Theron, Y.-C. Wu, S.-K. Lai, C.-C. Liu, H.-Y. Lei, An interferon-gamma-related cytokine storm in SARS patients. *J. Med. Virol.* **75**, 185–194 (2005).

29. X. Yang, X. Cheng, Y. Tang, X. Qiu, Z. Wang, G. Fu, J. Wu, H. Kang, J. Wang, H. Wang, F. Chen, X. Xiao, T. R. Billiar, B. Lu, The role of type 1 interferons in coagulation induced by gram-negative bacteria. *Blood* **135**, 1087–1100 (2020).

30. F. J. Sorrell, M. Szklarz, K. R. Abdul Azeez, J. M. Elkins, S. Knapp, Family-wide structural analysis of human numb-associated protein kinases. *Structure* **24**, 401–411 (2016).

31. S. Ottaviani, J. Stebbing, What is the best drug to treat COVID-19? The need for randomized controlled trial. *Med. (N.Y.)*, https://doi.org/10.1016/j.medj.2020.04.002 (2020).

32. S. Lo Caputo, G. Corso, M. Clerici, T. A. Santantonio, Baricitinib: A chance to treat COVID-19? *J. Med. Virol.* **2020**, (2020).

33. J. Nikolich-Zugich, K. S. Knox, C. T. Rios, B. Natt, D. Bhattacharya, M. J. Fain, SARS-CoV-2 and COVID-19 in older adults: What we may expect regarding pathogenesis, immune responses, and outcomes. *GeroSci.* **42**, 505–514 (2020).

34. C. G. K. Ziegler, S. J. Allon, S. K. Nyquist, I. M. Mbano, V. N. Miao, C. N. Tzouanas, Y. Cao, A. S. Yousif, J. Bals, B. M. Hauser, J. Feldman, C. Muus, M. H. Wadsworth II, S. W. Kazer, T. K. Hughes, B. Doran, G. J. Gatter, M. Vukovic, F. Taliaferro, B. E. Mead, Z. Guo, J. P. Wang, D. Gras, M. Plaisant, M. Ansari, I. Angelidis, H. Adler, J. M. S. Sucre, C. J. Taylor, B. Lin, A. Waghray, V. Mitsialis, D. F. Dwyer, K. M. Buchheit, J. A. Boyce, N. A. Barrett, T. M. Laidlaw, S. L. Carroll, L. Colonna, V. Tkachev, C. W. Peterson, A. Yu, H. B. Zheng, H. P. Gideon, C. G. Winchell, P. L. Lin, C. D. Bingle, S. B. Snapper, J. A. Kropski, F. J. Theis, H. B. Schiller, L.-E. Zaragosi, P. Barbry, A. Leslie, H.-P. Kiem, J. A. L. Flynn, S. M. Fortune, B. Berger, R. W. Finberg, L. S. Kean, M. Garber, A. G. Schmidt, D. Lingwood, A. K. Shalek, J. Ordovas-Montanes; HCA Lung Biological Network, SARS-CoV-2 receptor ACE2 is an interferon-stimulated gene in human airway epithelial cells and is detected in specific cell subsets across tissues. *Cell* **181**, 1016–1035.e19 (2020).

35. C. Zhang, L. Shi, F.-S. Wang, Liver injury in COVID-19: Management and challenges. *Lancet* **5**, 428–430 (2020).

36. Q. Zhang, P. Bastard, Z. Liu, J. le Pen, M. Moncada-Velez, J. Chen, M. Ogishi, I. K. D. Sabli, S. Hodeib, C. Korol, J. Rosain, K. Bilguvar, J. Ye, A. Bolze, B. Bigio, R. Yang, A. A. Arias, Q. Zhou, Y. Zhang, F. Onodi, S. Korniotis, L. Karpf, Q. Philippot, M. Chbihi, L. Bonnet-Madin, K. Dorgham, N. Smith, W. M. Schneider, B. S. Razooky, H. H. Hoffmann, E. Michailidis, L. Moens, J. E. Han, L. Lorenzo, L. Bizien, P. Meade, A. L. Neehus, A. C. Ugurbil, A. Corneau, G. Kerner, P. Zhang, F. Rapaport, Y. Seeleuthner, J. Manry, C. Masson, Y. Schmitt, A. Schlüter, T. le Voyer, T. Khan, J. Li, J. Fellay, L. Roussel, M. Shahrooei, M. F. Alosaimi, D. Mansouri, H. al-Saud, F. al-Mulla, F. Almourfi, S. Z. al-Muhsen, F. Alsohime, S. al Turki, R. Hasanato, D. van de Beek, A. Biondi, L. R. Bettini, M. D'Angio', P. Bonfanti, L. Imberti, A. Sottini, S. Paghera, E. Quiros-Roldan, C. Rossi, A. J. Oler, M. F. Tompkins, C. Alba, I. Vandernoot, J. C. Goffard, G. Smits, I. Migeotte, F. Haerynck, P. Soler-Palacin, A. Martin-Nalda, R. Colobran, P. E. Morange, S. Keles, F. Çölkesen, T. Ozcelik, K. K. Yasar, S. Senoglu, Ş. N. Karabela, C. Rodríguez-Gallego, G. Novelli, S. Hraiech, Y. Tandjaoui-Lambiotte, X. Duval, C. Laouénan; COVID-STORM Clinicians; COVID Clinicians; Imagine COVID Group; French COVID Cohort Study Group; CoV-Contact Cohort; Amsterdam UMC Covid-19 Biobank; COVID Human Genetic Effort; NIAID-USUHS/TAGC COVID Immunity Group, A. L. Snow, C. L. Dalgard, J. D. Milner, D. C. Vinh, T. H. Mogensen, N. Marr, A. N. Spaan, B. Boisson, S. Boisson-Dupuis, J. Bustamante, A. Puel, M. J. Ciancanelli, I. Meyts, T. Maniatis, V. Soumelis, A. Amara, M. Nussenzweig, A. García-Sastre, F. Krammer, A. Pujol, D. Duffy, R. P. Lifton, S. Y. Zhang, G. Gorochov, V. Béziat, E. Jouanguy, V. Sancho-Shimizu, C. M. Rice, L. Abel, L. D. Notarangelo, A. Cobat, H. C. Su, J. L. Casanova, Inborn errors of type I IFN immunity in patients with life-threatening COVID-19. *Science* **370**, eabd4570 (2020).

37. Z. Zhou, L. Ren, L. Zhang, J. Zhong, Y. Xiao, Z. Jia, L. Guo, J. Yang, C. Wang, S. Jiang, D. Yang, G. Zhang, H. Li, F. Chen, Y. Xu, M. Chen, Z. Gao, J. Yang, J. Dong, B. Liu, X. Zhang, W. Wang, K. He, Q. Jin, M. Li, J. Wang, Heightened innate immune responses in the respiratory tract of COVID-19 patients. *Cell Host Microbe* **27**, 883–890.e2 (2020).

38. I. Hamming, W. Timens, M. L. C. Bulthuis, A. T. Lely, G. J. Navis, H. van Goor, Tissue distribution of ACE2 protein, the functional receptor for SARS coronavirus. A first step in understanding SARS pathogenesis. *J. Pathol.* **203**, 631–637 (2004).

39. H. Jia, C. Thelwell, P. Dilger, C. Bird, S. Daniels, M. Wadhwa, Endothelial cell functions impaired by interferon in vitro: Insights into the molecular mechanism of thrombotic microangiopathy associated with interferon therapy. *Thromb. Res.* **163**, 105–116 (2018).

40. M. M. Lamers, J. Beumer, J. van der Vaart, K. Knoops, J. Puschhof, T. I. Breugem, R. B. G. Ravelli, J. P. van Schayck, A. Z. Mykytyn, H. Q. Duimel, E. van Donselaar, S. Riesebosch, H. J. H. Kuijpers, D. Schipper, W. J. van de Wetering, M. de Graaf, M. Koopmans, E. Cuppen, P. J. Peters, B. L. Haagmans, H. Clevers, SARS-CoV-2 productively infects human gut enterocytes. *Science* **369**, 50–54 (2020).

41. N. Vilarnau, S. U. Vorrink, M. Ingelman-Sundberg, V. M. Lauschke, A 3D cell culture model identifies Wnt/β-catenin mediated inhibition of p53 as a critical step during human hepatocyte regeneration. *Adv. Sci.* **7**, 2000248 (2020).

42. G. Paizis, C. Tikellis, M. E. Cooper, J. M. Schembri, R. A. Lew, A. I. Smith, T. Shaw, F. J. Warner, A. Zuilli, L. M. Burrell, P. W. Angus, Chronic liver injury in rats and humans upregulates the novel enzyme angiotensin converting enzyme 2. *Gut* **54**, 1790–1796 (2005).

43. M. Levi, J. Thachil, T. Iba, J. H. Levy, Coagulation abnormalities and thrombosis in patients with COVID-19. *Lancet Haematol.* **7**, e438–e440 (2020).

44. I. C. Scott, S. L. Hider, D. L. Scott, Thromboembolism with Janus kinase (JAK) inhibitors for rheumatoid arthritis: How real is the risk? *Drug Saf.* **41**, 645–653 (2018).

45. P. J. Richardson, S. Ottaviani, A. Prelle, J. Stebbing, G. Casalini, M. Corbellino, CNS penetration of potential anti-COVID-19 drugs. *J. Neurol.* **267**, 1880–1882 (2020).

46. C. Gavegnano, W. B. Haile, S. Hurwitz, S. Tao, Y. Jiang, R. F. Schinazi, W. R. Tyor, Baricitinib reverses HIV-associated neurocognitive disorders in a SCID mouse model and reservoir seeding in vitro. *J. Neuroinflammation* **16**, 182 (2019).

47. J. Zhong, J. Tang, C. Ye, L. Dong, The immunology of COVID-19: Is immune modulation an option for treatment? *Lancet Rheumatol.* , (2020).

48. M. Hoffmann, H. Kleine-Weber, S. Schroeder, N. Krüger, T. Herrler, S. Erichsen, T. S. Schiergens, G. Herrler, N.-H. Wu, A. Nitsche, M. A. Müller, C. Drosten, S. Pöhlmann, SARS-CoV-2 cell entry depends on ACE2 and TMPRSS2 and is blocked by a clinically proven protease inhibitor. *Cell* **81**, 271–280.e8 (2020).

49. F. Handle, M. Puhr, G. Schaefer, N. Lorito, J. Hoefer, M. Gruber, F. Guggenberger, F. R. Santer, R. B. Marques, W. M. van Weerden, F. Claessens, H. H. H. Erb, Z. Culig, The STAT3 inhibitor galiellalactone reduces IL6-mediated AR activity in benign and malignant prostate models. *Mol. Cancer Ther.* **17**, 2722–2731 (2018).

50. D. E. Ho, K. Imai, G. King, E. A. Stuart, Matching as nonparametric preprocessing for reducing model dependence in parametric causal inference. *Polit. Anal.* **15**, 199–236 (2007).

51. C. C. Bell, D. F. G. Hendriks, S. M. L. Moro, E. Ellis, J. Walsh, A. Renblom, L. F. Puigvert, A. C. A. Dankers, F. Jacobs, J. Snoeys, R. L. Sison-Young, R. E. Jenkins, Å. Nordling, S. Mkrtchian, B. K. Park, N. R. Kitteringham, C. E. P. Goldring, V. M. Lauschke, M. Ingelman-Sundberg,

Characterization of primary human hepatocyte spheroids as a model system for drug-induced liver injury, liver function and disease. *Sci. Rep.* **6**, 25187 (2016).

52. C. C. Bell, V. M. Lauschke, S. U. Vorrink, H. Palmgren, R. Duffin, T. B. Andersson, M. Ingelman-Sundberg, Transcriptional, functional, and mechanistic comparisons of stem cell-derived hepatocytes, HepaRG cells, and three-dimensional human hepatocyte spheroids as predictive in vitro systems for drug-induced liver injury. *Drug Metab. Dispos.* **45**, 419–429 (2017).

53. S. U. Vorrink, S. Ullah, S. Schmidt, J. Nandania, V. Velagapudi, O. Beck, M. Ingelman-Sundberg, V. M. Lauschke, Endogenous and xenobiotic metabolic stability of primary human hepatocytes in long-term 3D spheroid cultures revealed by a combination of targeted and untargeted metabolomics. *FASEB J.* **31**, 2696–2708 (2017).

54. V. Monteil, H. Kwon, P. Prado, A. Hagelkrüys, R. A. Wimmer, M. Stahl, A. Leopoldi, E. Garreta, C. H. del Pozo, F. Prosper, J. P. Romero, G. Wirnsberger, H. Zhang, A. S. Slutsky, R. Conder, N. Montserrat, A. Mirazimi, J. M. Penninger, Inhibition of SARS-CoV-2 infections in engineered human tissues using clinical-grade soluble human ACE2. *Cell* **181**, 905–913.e7 (2020).

55. E. F. Pettersen, T. D. Goddard, C. C. Huang, G. S. Couch, D. M. Greenblatt, E. C. Meng, T. E. Ferrin, UCSF Chimera—A visualization system for exploratory research and analysis. *J. Comput. Chem.* **25**, 1605–1612 (2004).

Citation: J. Stebbing, G. Sánchez Nievas, M. Falcone, S. Youhanna, P. Richardson, S. Ottaviani, J. X. Shen, C. Sommerauer, G. Tiseo, L. Ghiadoni, A. Virdis, F. Monzani, L. R. Rizos, F. Forfori, A. Avendaño Céspedes, S. De Marco, L. Carrozzi, F. Lena, P. M. Sánchez-Jurado, L. G. Lacerenza, N. Cesira, D. Caldevilla Bernardo, A. Perrella, L. Niccoli, L. S. Méndez, D. Matarrese, D. Goletti, Y.-J. Tan, V. Monteil, G. Dranitsaris, F. Cantini, A. Farcomeni, S. Dutta, S. K. Burley, H. Zhang, M. Pistello, W. Li, M. M. Romero, F. Andrés Pretel, R. S. Simón-Talero, R. García-Molina, C. Kutter, J. H. Felce, Z. F. Nizami, A. G. Miklosi, J. M. Penninger, F. Menichetti, A. Mirazimi, P. Abizanda, V. M. Lauschke, JAK inhibition reduces SARS-CoV-2 liver infectivity and modulates inflammatory responses to reduce morbidity and mortality. *Sci. Adv.* **7**, eabe4724 (2021).

ScienceAdvances

JAK inhibition reduces SARS-CoV-2 liver infectivity and modulates inflammatory responses to reduce morbidity and mortality

Justin StebbingGinés Sánchez NievasMarco FalconeSonia YouhannaPeter RichardsonSilvia OttavianiJoanne X. ShenChristian SommerauerGiusy TiseoLorenzo GhiadoniAgostino VirdisFabio MonzaniLuis Romero RizosFrancesco ForforiAlmudena Avendaño CéspedesSalvatore De MarcoLaura CarrozziFabio LenaPedro Manuel Sánchez-JuradoLeonardo Gianluca LacerenzaNencioni CesiraDavid Caldevilla BernardoAntonio PerrellaLaura NiccoliLourdes Sáez MéndezDaniela MatarreseDelia GolettiYee-Joo TanVanessa MonteilGeorge DranitsarisFabrizio CantiniAlessio FarcomeniShuchismita DuttaStephen K. BurleyHaibo ZhangMauro PistelloWilliam LiMarta Mas RomeroFernando Andrés PretelRafaela Sánchez Simón-TaleroRafael García-MolinaClaudia KutterJames H. FelceZehra F. NizamiAndras G. MiklosiJosef M. PenningerFrancesco MenichettiAli MirazimiPedro AbizandaVolker M. Lauschke

View the article online
https://www.science.org/doi/10.1126/sciadv.abe4724
Permissions
https://www.science.org/help/reprints-and-permissions

Use of this article is subject to the Terms of service